Nanoscale

RSC Publishing

PAPER

Band structure quantization in nanometer sized ZnO clusters†

Cite this: *Nanoscale*, 2013, **5**, 3757

Koen Schouteden,*[a] Yu-Jia Zeng,[a] Koen Lauwaet,[a] Christian P. Romero,‡[a] Bart Goris,[b] Sara Bals,*[b] Gustaaf Van Tendeloo,[b] Peter Lievens[a] and Chris Van Haesendonck[a]

Received 7th December 2012
Accepted 27th February 2013

DOI: 10.1039/c3nr33989k

www.rsc.org/nanoscale

Nanometer sized ZnO clusters are produced in the gas phase and subsequently deposited on clean Au(111) surfaces under ultra-high vacuum conditions. The zinc blende atomic structure of the approximately spherical ZnO clusters is resolved by high resolution scanning transmission electron microscopy. The large band gap and weak n-type conductivity of individual clusters are determined by scanning tunnelling microscopy and spectroscopy at cryogenic temperatures. The conduction band is found to exhibit clear quantization into discrete energy levels, which can be related to finite-size effects reflecting the zero-dimensional confinement. Our findings illustrate that gas phase cluster production may provide unique possibilities for the controlled fabrication of high purity quantum dots and heterostructures that can be size selected prior to deposition on the desired substrate under controlled ultra-high vacuum conditions.

1 Introduction

The continued scientific and technological interest in the II–VI compound semiconductor ZnO is related to its broad range of applicable properties, including piezoelectricity, high transparency, high electron mobility, large direct band gap around 3.4 eV and strong room-temperature luminescence due to its large exciton binding energy (about 60 meV).[1,2] Moreover, scaling ZnO structures down to the nanometer scale, *i.e.* to low-dimensional electronic systems, may further improve and even allow tuning of the properties due to the occurrence of quantum size effects. The majority of the fabrication routes of ZnO material with reduced dimensionality, including quantum dots, nanocrystals, nanowires and thin films, typically involves the use of chemical solutions and/or exposure to ambient environment conditions,[1–4] during which (a certain degree of) contamination and inhomogeneity cannot be avoided. Contaminants may result in chemical doping and hence mask its intrinsic properties. In order to reliably unravel the intrinsic properties of ZnO nanostructures, preparation and characterization techniques under ultra-high vacuum (UHV) are of crucial importance. Here, we focus on nanometer sized ZnO clusters that are prepared, deposited and characterized under controlled conditions in UHV.

When all three dimensions become comparable to or smaller than the bulk ZnO exciton Bohr radius $a_B \approx 2.3$ nm,[5] ZnO nanoparticles can be considered as zero-dimensional (0D) "artificial atoms". Such nanoparticles yield major perspectives for novel applications in *e.g.* quantum dots of a (diluted) magnetic semiconductor,[6–8] solar cells,[9] and field emitters.[10] On the other hand, at the nanometer scale the smallest difference in particle size may give rise to very different electronic properties due to the dominant finite size effects. These effects are much more pronounced for semiconducting nanoparticles than for metallic nanoparticles.[11,12] For a spherical semiconductor particle of radius R both the (top of the) valence band and the (bottom of the) conduction band experience quantization and the resulting series of size dependent discrete energy levels E_{nl}, which are accompanied by atom-like envelope wave function symmetries (s, p, d,…), can be described by:[11,12]

$$E_{nl} = \frac{0.377\ \text{eV}}{(m^*/m_e)R^2}\ \frac{{\beta_{nl}}^2}{{\beta_0}^2}\ \ n,\ l = 1, 2, 3, \ldots, \qquad (1)$$

where m^* is the (valence/conduction) effective mass and β_{nl} is the n^{th} zero of the l^{th} spherical Bessel function. Area-averaging measurements such as photoluminescence and absorption measurements[1,3] of an ensemble or film of nanoparticles yield a smoothed average of the size dependent properties of these particles and valuable information on the individual particle properties is lost. Local probing techniques are clearly required. High angle annular dark field scanning transmission electron microscopy (HAADF-STEM)[13–15] is able to resolve the atomic

[a]*Laboratory of Solid-State Physics and Magnetism, KU Leuven, Celestijnenlaan 200d – box 2414, BE-3001 Leuven, Belgium. E-mail: Koen.Schouteden@fys.kuleuven.be; Fax: +32 16 327983; Tel: +32 16 327245*

[b]*EMAT, University of Antwerp, Groenenborgerlaan 171, BE-2020 Antwerp, Belgium. E-mail: Sara.Bals@ua.ac.be*

† Electronic supplementary information (ESI) available. See DOI: 10.1039/c3nr33989k

‡ Present address: Departamento de Física, Universidad de Santiago de Chile, Av. Ecuador 3493, Estación Central, Santiago, Chile.

structure of individual nanoparticles, while scanning tunnelling microscopy (STM) combined with scanning tunnelling spectroscopy (STS) allows for systematic investigation of the electronic properties at the level of individual nanoparticles with high spatial and energy resolution. STM and STS have been successfully applied to a broad variety of semiconductor nanoparticles, including CdSe,[16–18] PbSe[17] and InAs.[19,20] So far, however, STM and STS investigations of ZnO have been rather scarce and have been limited to thin films and bulk crystals.[21–24] Detailed STM and STS investigations of gas phase clusters that are deposited and studied under UHV conditions have remained very limited as well.[25–30]

Here, we report direct evidence of pronounced quantization of the electronic band structure of individual nanometer sized ZnO clusters on Au(111) surfaces. ZnO clusters are prepared under controlled conditions using a UHV laser vaporization source, after which the clusters are deposited on clean Au(111) surfaces. The zinc blende atomic structure of the spherical ZnO clusters is visualized by means of HAADF-STEM imaging. STM and STS measurements reveal the large band gap between the valence and conduction band of the clusters. Due to the finite size of the clusters, the band structure is expected to split up in a series of discrete energy levels. This is schematically illustrated in Fig. 1, where a metallic STM tip is placed in tunnel contact with a ZnO cluster. Since the clusters are in direct electrical contact with the metallic substrate, the electron tunnelling rate between the STM tip and the cluster is much smaller than that between the cluster and the substrate. Hence, tunnelling electrons cannot accumulate in the cluster, implying that charging effects and related electron–electron interaction effects in the cluster are limited. This is somewhat similar to the case of so-called *shell-tunnelling* STS where the nanoparticle is the central island of a double-barrier tunnel junction.[16–18] Resonances in the STS spectra therefore reflect the discrete single-electron density of states of the clusters. As discussed in detail below, the splitting up of the band structure can be observed clearly only for the conduction band.

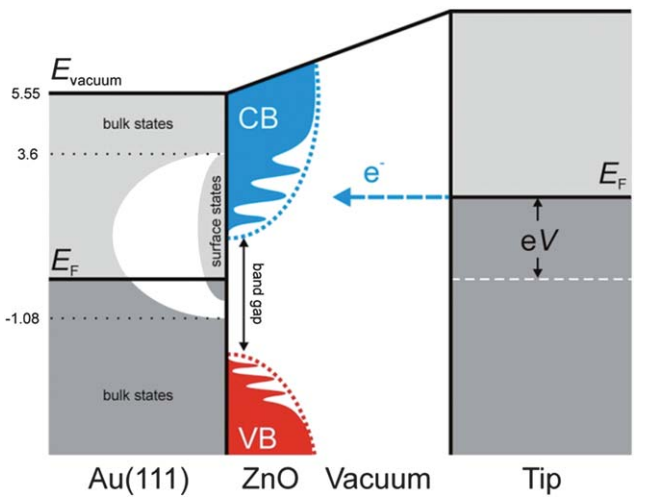

Fig. 1 Schematic energy diagram of an STM tip in tunnel contact with a nanometer sized ZnO cluster on a Au(111) surface at a positive sample voltage *V*. The ZnO valence band (VB) and conduction band (CB), separated from each other by a large band gap, become quantized because of the small size of the cluster. The Au(111) surface exhibits a gap in its projected bulk band structure that accommodates the Au(111) surface state. Indicated energies are with respect to the Fermi level E_F and are taken from ref. 31.

2 Experimental section

2.1 Deposition of gas phase ZnO clusters on clean Au(111)

Clean atomically flat Au(111) films are prepared as described in ref. 28 and are transported between the cluster deposition apparatus and the STM setup by means of a home-built UHV transport vessel (pressure in the 10^{-10} mbar range). ZnO clusters are produced in a laser vaporization source.[32] By ablating pure Zn followed by thermalization of the hot Zn atoms in a $He–O_2$ mixture (10% O_2, impurity level < 1 ppm) we obtain pure ZnO clusters that are deposited onto Au(111) at room temperature in an integrated UHV deposition chamber. The ratio of O_2 to Zn in the ablation stage is well above 10 : 1, *i.e.* for every impact with an incoming Zn atom of a growing cluster in the formation process there occur more than 10 impacts with O_2. As we will show below, our HAADF-STEM and STM–STS measurements confirm the high structural quality of the produced ZnO clusters. Cluster beams with a size distribution ranging from a few atoms up to several hundreds of atoms can be produced. The clusters are deposited with their inherent low kinetic energy (around 0.1 eV per atom) and consequently negligible cluster deformation will occur upon impact. Deposition times were chosen to achieve a low cluster density well below complete coverage of the substrate, which can be monitored by a quartz microbalance.

2.2 Cryogenic STM and STS measurements

STM and STS measurements are performed with an UHV (base pressure in the 10^{-11} mbar range) STM setup (Omicron Nanotechnology) at 4.5 K. Electrochemically etched W tips and mechanically cut PtIr (10% Ir) tips are cleaned *in situ* as described in ref. 33. Spectra of d*I*/d*V versus V* (*V* is the voltage applied to the sample, while the STM tip is virtually grounded) are acquired with open and closed feedback loops *via* lock-in detection at a modulation frequency of 840 Hz and with a sample voltage modulation amplitude in the 10 to 50 mV range. Image processing is performed using Nanotec WSxM.[34]

2.3 HAADF-STEM imaging

HAADF-STEM imaging[15,35] is carried out using a FEI Titan 50–80 microscope operating at a relatively low accelerating voltage of 120 kV. For this purpose ZnO clusters are deposited on a copper supported carbon TEM grid in the cluster deposition apparatus, after which the samples are transported under ambient conditions to the electron microscope. The ZnO clusters are found to reveal dynamic behavior under the electron beam related to knock-on energy transfer. For this reason STEM images are acquired using relatively short acquisition times (0.8 s per frame).

3 Results and discussion

3.1 Morphology and atomic structure of the deposited ZnO clusters

After deposition, the majority of the ZnO clusters are found to be well separated from each other, while only a minor fraction of the clusters make contact with each other or are in close proximity of each other. STM images before and after annealing up to around 770 K reveal a similar fraction of individual clusters on the Au(111) surface, indicating that the deposited clusters do not diffuse at these annealing temperatures. The STM and STS data presented below are obtained after optimizing the measurement stability by annealing the sample to moderate temperatures around 470 K to remove molecular adsorbates that are adsorbed on the Au(111) surface during the ZnO cluster production and deposition process.

Fig. 2(a) presents the STM topography image of multiple ZnO nanoclusters on Au(111). The clusters (indicated by white arrows) are randomly spread across the atomically flat terraces of the Au(111) surface, indicating that they are pinned upon deposition so that diffusion is avoided. Indeed, the clusters do not reveal any preferential positioning, *e.g.* at Au(111) step edges or at atomic size defects that exist at the elbows of the herringbone reconstructed surface.[36] Upon more careful inspection of Fig. 2(a), a relatively large amount of atomic sized particles can be discerned. These particles are atomic sized ZnO clusters that are also present in the deposited cluster beam. Atomic sized clusters typically exhibit a limited mobility on atomically flat surfaces, allowing them to form small aggregates *e.g.* at surface defects and at the elbows of the Au(111) herringbone reconstruction (see *e.g.* ref. 28). In this work we focus on the larger clusters that do not show any significant mobility on the Au(111) surface. These larger ZnO clusters have heights up to 4 nm. Note that due to unavoidable convolution of the STM tip shape with the ZnO cluster shape, the clusters appear significantly broadened in STM topography images and the diameter of the clusters can hence not be accurately determined.[28] On the other hand, the height of the clusters is not influenced by convolution effects and can be determined with sub-angstrom precision at low temperatures. The height histogram in Fig. 2(b), which is based on a series of STM topography images such as the one in Fig. 2(a), reveals that the average cluster height (= cluster diameter, assuming a spherical cluster shape) is 2.5 nm. This is comparable to the ZnO Bohr radius $a_B \approx 2.3$ nm,[5] implying the ZnO clusters enter the so-called *strong confinement regime* and finite-size effects can be expected to dominate the electronic properties. In view of future experiments and applications, we would like to note that it is possible to select clusters with a specific size from the cluster beam *via* mass-selection with *e.g.* a quadrupole or time-of-flight mass selector.[25,29,37,38] Here, we aim at investigating the electronic behavior of the ZnO clusters with varying size and hence we did not size select the cluster prior deposition on the Au(111) substrate. Exceptionally, a cluster exhibiting hexagonal facets is observed (see inset in Fig. 2(a)). Typically, however, clusters do not have a pronounced polygonal shape in STM topography images, which indicates that the random orientation of the clusters relative to the Au(111) surface after deposition was pinned upon impact on the substrate.

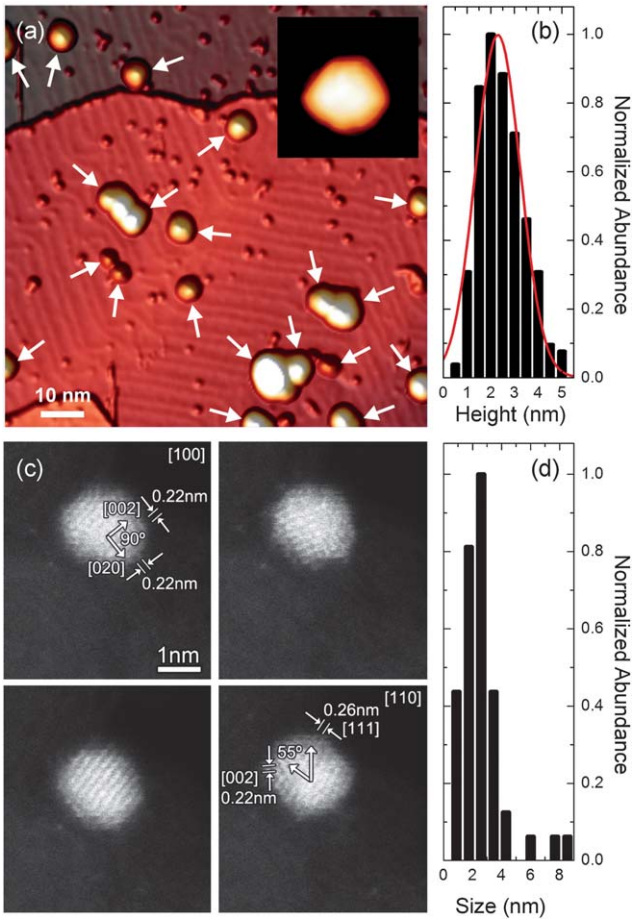

Fig. 2 (a) STM topography image of preformed ZnO nanoclusters deposited on clean Au(111) (color height scale = 2.9 nm, $I = 0.1$ nA, $V = 2.5$ V). White arrows indicate the investigated ZnO clusters. Inset: 11 × 11 nm^2 close-up view of a ZnO cluster with hexagonal shape (color height scale = 1.6 nm, $I = 0.5$ nA, $V = 2.0$ V). (b) Height histogram of the deposited clusters on Au(111) as determined from height profiles of a series of STM topography measurements comprising 246 clusters. Average cluster height is 2.5 ± 0.9 nm. The red solid line is a Gaussian fit of the histogram bar heights. (c) Series of HAADF-STEM images of a ZnO nanoparticle with a diameter of about 2 nm. A transition is observed from the [100] (upper left image) to the [110] (lower right image) zone axis in the zinc blende structure. The crystal facets, the lattice distance, and the angle between two crystal facets are indicated for the two different cluster orientations in the upper left and lower right images. (d) Size histogram of the deposited clusters as determined from a series of HAADF-STEM images comprising 49 clusters. Average cluster diameter is 2.6 ± 1.6 nm.

As already indicated above, due to STM tip convolution effects, the atomic structure of a ZnO cluster cannot be clearly resolved relying on STM. Therefore, HAADF-STEM imaging[35] is performed to visualize the atomic structure of the ZnO clusters. For this purpose gas phase ZnO clusters are deposited on carbon TEM grids. The approximately spherical ZnO nanoparticles are found to reveal dynamic behavior during TEM investigation because of knock-on energy transfer from the electron beam. This indicates that the clusters largely retain their spherical shape after deposition and that they experience negligible deformation upon impact. For this reason

HAADF-STEM images are acquired with relatively short acquisition times of 0.8 s per frame. We found that ZnO clusters exhibit a zinc blende crystalline structure instead of the wurtzite structure of bulk ZnO; the wurtzite structure has been observed before for ZnO nanoparticles with diameters in the 1 to 6 nm range.[1] This difference may be related to the very different preparation routes that are involved, *i.e.* preparation under vacuum conditions or in chemical solution.

A series of subsequently recorded HAADF-STEM images of an individual ZnO cluster is presented in Fig. 2(c), indicating a transformation of the cluster orientation from the [100] zone axis (top left) to the [110] zone axis (bottom right). More HAADF-STEM images are presented in Fig. S1 in the ESI.† In Fig. 2(d) we present a size histogram of ZnO clusters based on HAADF-STEM data such as the image in Fig. 2(c). The histogram reveals a Gaussian-like distribution with an average cluster diameter of 2.6 ± 1.6 nm, which is very similar to the STM-based cluster height histogram in Fig. 2(b). This confirms that the clusters retain to a large extent their approximately spherical shape on Au(111) as well. The bottom right HAADF-STEM image of the zinc blende ZnO cluster in Fig. 2(c) has a hexagonal contour similar to the ZnO cluster in the STM image presented in the inset in Fig. 2(a), which appears broadened due to tip convolution effects. The fact that the clusters retain to a large extent their spherical shape after deposition on Au(111) as well as on carbon TEM grids indicates that the ZnO clusters are likely to have a zinc blende structure on Au(111) as well. However, as the clusters are deposited on different substrates, the latter statement should be taken with caution.

3.2 Band structure quantization of the deposited ZnO clusters

$I(V)$ spectra on single ZnO clusters always reveal a large band gap in the 3 to 3.5 eV range that is asymmetric with respect to the Fermi level E_F at $V = 0$ (see Fig. 3(a)). This gap size is comparable to the known band gap of (bulk) ZnO,[2] *i.e.* 3.4 eV, and indicates the high quality of the ZnO clusters. Minor variations of the gap size in subsequently recorded spectra (see Fig. 3(a)) are related to measurement instabilities that occur at these relatively high voltages, *e.g.* due to the displacement of an atom at the tip apex. The observed band gap of the ZnO clusters spans from 0.5 to 1.0 eV above E_F to −2.0 to −2.5 eV below E_F (Fig. 3(a)). ZnO clusters hence possess weak n-type conductivity, which is also typically observed for ZnO films and bulk ZnO material. The n-type conductivity of ZnO has been linked to the presence of zinc interstitials and oxygen vacancies.[39] More recently the n-type conductivity has been attributed to the presence of hydrogen (substituting an oxygen atom and equally bonding to all four Zn neighbors).[40]

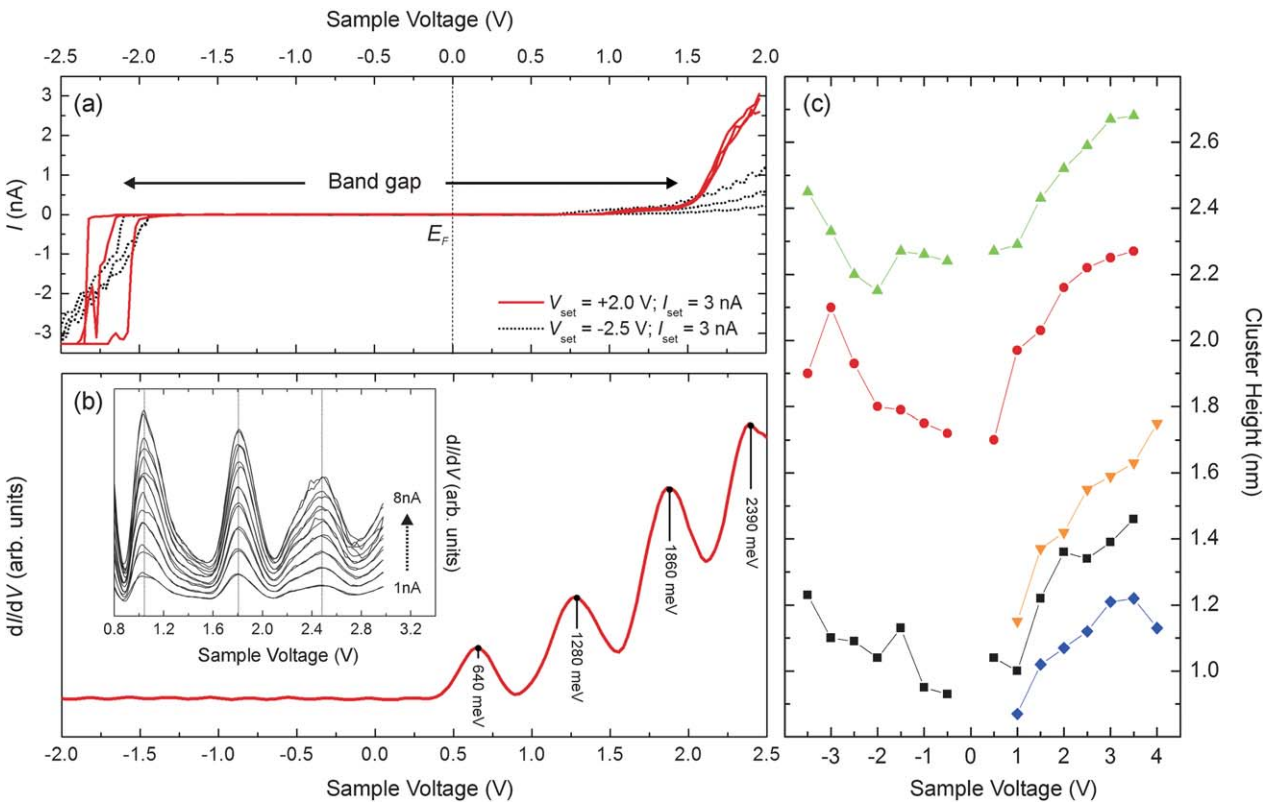

Fig. 3 (a) $I(V)$ spectra successively recorded on an individual ZnO cluster at the indicated tunnelling conditions (open feedback loop), revealing a large band gap in the 3 to 3.5 eV range with the Fermi level E_F located closer to the conduction band than to the valence band. (b) Typical (dI/dV)(V) spectrum recorded on another individual ZnO cluster, revealing pronounced quantization of the ZnO conduction band (I = 3.0 nA, V = 2.5 V, open feedback loop). Inset: (dI/dV)(V) spectra recorded on an individual ZnO cluster at different settings of the tunnelling current (V = 3.0 V, closed feedback loop). (c) Dependence of the cluster height observed in STM topography images on the applied sample voltage. Each label corresponds to a different ZnO cluster.

Next, the electronic structure of the ZnO clusters is probed in more detail by recording $(dI/dV)(V)$ spectra that reflect the local density of states (LDOS). A typical spectrum is presented in Fig. 3(b) (cluster height is about 1.4 nm). It is found that all investigated ZnO clusters exhibit a series of pronounced resonances in the empty state region (positive sample voltage V) where $I(V)$ spectra reveal a strong increase of the tunnelling current I. Additional STS data are presented in Fig. S2 in the ESI.† Because of the direct contact between the cluster and the Au(111) substrate, charging effects are absent and resonant peaks in the STS spectra reflect the single-electron density of states of the clusters[16–18] and can be attributed to discrete energy levels of the cluster. Energy separations are typically of the order of 100 meV for clusters in the here investigated size range. We can hence conclude that the conduction band of the ZnO clusters experiences quantization due to the finite size of the clusters,[11] as is illustrated in Fig. 1. In terms of the idealized model described by eqn (1) the four maxima observed in Fig. 3(b) may be addressed to the 1s (*i.e.* the lowest unoccupied molecular orbital), the 1p, the 1d and the 2s energy level or orbital of the 0D ZnO cluster.[12] In this view it can be expected that the intensity of the 2nd resonant state in Fig. 3(b) is about 3 times higher than that of the 1st resonant state because of the threefold degeneracy of the p-state (*i.e.* p_x, p_y and p_z). The intensity of the 2nd state is indeed significantly larger, *i.e.* about 2 times larger than that of the 1st state, yet smaller than expected. This discrepancy is commonly observed for semiconductor nanoparticles and is related to the smaller contribution of the p_x and p_y orbitals (smaller transmission coefficient) at the centre of the cluster when compared to the s orbital and p_z orbital.[17,18] A similar reasoning applies for the states at higher energies. We note, however, that because of the possible deviation of the cluster shape from spherical symmetry as well as interaction with the underlying Au(111) substrate, this "labelling" should be taken with care.

Assuming a spherical particle shape and taking the conduction effective mass $m^* \approx 0.2$–$0.3\ m_e$,[1,3,41] eqn (1) predicts energy separations of the order of 100 meV for particles with a diameter of 4 nm, up to a few eV for nanoparticles with a diameter of 1 nm. These observed energy separations are typically smaller than those predicted by eqn (1). This may be attributed to (voltage dependent, see below) deviations of the cluster shape from the "ideal" spherical shape that is assumed when deriving eqn (1). Furthermore, coupling of the cluster to the metallic Au(111) substrate allows (vertical) transport of electrons between cluster and substrate so that electrons are only confined laterally, *i.e.* in two dimensions rather than in three dimensions. Indeed, the (relatively) broad width of the resonances in Fig. 3(b) (in the 200–300 meV range) when compared to semiconductor nanoparticles that are isolated from the surface by a thin molecular layer (typically below 100 meV (ref. 16 and 17)) is indicative of significant coupling between the semiconducting cluster and the metallic substrate.

We observed that the quantized energies are sensitive to the precise geometry of the STM tip apex (data not shown). Maxima occur at somewhat different energies after a "tip change" that occasionally occurs during scanning of the sample surface, which may be related to an altered sensitivity of the STM tip for states with a different parallel component $k_{||}$ of the wave vector $\boldsymbol{k}$.[42,43] A clear dependence of the energy separations between the successive quantized energy levels on the cluster size (*i.e.* the cluster height) could not be identified, which can be related to the sensitivity of the observed energy maxima to possible "tip changes". Alternatively, Liljeroth *et al.* previously addressed observed variations between subsequently recorded STS spectra on a semiconductor nanoparticle to (uncontrolled) trapping of a charge in the surroundings of the nanoparticle.[16,17]

Considering the fact that the conduction band is quantized due to the small size of the ZnO clusters, the valence band is expected to reveal a similar quantization.[11,12] However, clear quantization could not be resolved in the negative voltage region by our STS measurements. This may be related to the measurement technique. First, since the Fermi level is located closer to the conduction band than to the valence band (see Fig. 3(a)), higher (in absolute values) sample voltage is required to probe the filled valence states regime of the cluster. These higher voltages are accompanied by an increased probability for measurement instabilities, hampering reliable measurements in this regime.[18] Second, whereas empty sample states are probed in the positive sample voltage region, empty tip states become increasingly important in the negative sample voltage region,[42] which may additionally hamper a clear measurement of the quantized valence band of the ZnO clusters. Moreover, the reason that clear quantization is not observed in the negative voltage region may be related to the larger effective hole mass for the valence band, *i.e.* a few times larger than the effective electron mass for the conduction band.[41] This implies that energy separations between successive quantized valence band states are expected to be a few times smaller than those between quantized conduction band states [eqn (1)]. Nevertheless, since the conduction band exhibits a clear quantization, it can be assumed that the valence band is quantized as well, with smaller energy separations between the successive discrete states, as illustrated in Fig. 1.

In contrast to the dependence of the quantized energy levels on the precise geometry of the STM tip apex, these states are not influenced by the applied electric field (tip-cluster separation) between the STM tip and the cluster. In the inset of Fig. 3(b) successive $(dI/dV)(V)$ measurements are presented which are recorded for different settings of the tunnelling current ranging from 1 to 8 nA (closed feedback loop). Multiple spectra are presented for each setting of the tunneling current, illustrating the higher stability of the spectra that is observed for measurements in a smaller voltage range when compared to the spectra in Fig. 3(a). It can be seen that the increased electric field does not induce a detectable Stark shift of the discrete levels towards higher energies and only the peak intensity increases. Based on this insensitivity we can exclude that image-potential states are at the origin of the observed states.[44] Image-potential states typically develop *above* surfaces that exhibit a (surface) band gap and are very sensitive to externally applied electric fields. The here observed quantized states are located outside of the ZnO band gap (Fig. 3(a)) and do not exhibit a field-dependent Stark shift. Also, the independence of the

quantized states on the tip-cluster separation (that is related to the tunnelling current setpoint) further confirms that tunnelling occurs similar to tunnelling in the so-called shell-tunnelling regime (due to the direct contact between the cluster and the Au(111) substrate).[16–18] The recorded LDOS hence reflects the single-electron LDOS of the cluster in the absence of Coulomb charging effects.

3.3 Bias voltage dependent STM imaging

Finally, we found that the height of the ZnO clusters as observed in STM topography images depends on the applied sample voltage *V*, while it does not depend on the tunnelling current setpoint in the investigated 0.1 to 10.0 nA range. Fig. 3(c) provides an overview of the measured heights of various clusters of different size at sample voltages between −4 V and +4 V. It can be seen that the cluster height increases more or less linearly with increasing sample voltage, both for negative and positive voltages. This dependence can be related to the strongly energy (and hence voltage) dependent electronic structure of the ZnO clusters discussed above, while the energy dependence of the Au(111) electronic structure is much less pronounced. With increasing voltage more and more states of the ZnO clusters become available for tunnelling. Using a fixed tunnelling current setpoint (closed feedback loop) implies that with increasing sample voltage the tip-sample distance increases more when scanning above the ZnO cluster than on the surrounding Au(111) surface, hence yielding an increasing cluster height with increasing sample voltage. Note that discontinuities in the (quasi-)linear voltage dependence are always accompanied by a "tip change" during scanning of the sample surface. As discussed above, this influences the energy at which the maxima of the quantized states are observed and hence also the measured cluster height in STM topography images.

4 Conclusion

In summary, by means of STM and STS we unravelled the electronic structure of individual nanometer sized ZnO clusters on Au(111). The structure of the ZnO clusters was investigated using advanced TEM. The clusters all exhibit a large band gap around 3 eV. The conduction band is found to be quantized in a series of discrete energy levels due to the finite size of the 0D clusters. Gas phase cluster production provides opportunities for the well controlled fabrication of high purity quantum dots and heterostructures[45,46] that eventually can be size selected prior to deposition on the desired substrate[25,29,37,38] under clean UHV conditions. In particular, this technique yields perspectives for the longstanding quest for high quality p-type ZnO nanoparticles as well as for the field of spintronics,[2,47] since controlled doping of ZnO clusters with one or more (magnetic) atoms can be achieved by using a dual-laser vaporization source.

Acknowledgements

This work was supported by the Science Foundation – Flanders (FWO Belgium) through project number G.0024.10N, the postdoctoral grant of K.S. and the doctoral grant of B.G. The authors acknowledge financial support from the Flemish Hercules 3 programme for large infrastructure. G.V.T. acknowledges support by the European Research Council under the 7th Framework Program (FP7), ERC grant number 246791 – COUNTATOMS.

Notes and references

1 A. Wood, M. Giersig, M. Hilgendorff, A. Vilas-Campos, L. M. Liz-Marzan and P. Mulvaney, *Aust. J. Chem.*, 2003, **56**, 1051.
2 U. Özgür, Y. I. Alivov, C. Liu, A. Teke, M. A. Reshchikov, S. Dogan, V. Avrutin, S.-J. Cho and H. Morkoç, *J. Appl. Phys.*, 2005, **98**, 041301.
3 K.-F. Lin, H.-M. Cheng, H.-C. Hsu, L.-J. Lin and W.-F. Hsieh, *Chem. Phys. Lett.*, 2005, **409**, 208.
4 Z. L. Wang, *ACS Nano*, 2008, **2**, 1987.
5 Y. Gu, I. L. Kuskovsky, M. Yin, S. O'Brien and G. F. Neumark, *Appl. Phys. Lett.*, 2004, **85**, 3833.
6 P. V. Radovanovic and D. R. Gamelin, *Phys. Rev. Lett.*, 2003, **91**, 157202.
7 N. S. Norberg, K. R. Kittilstved, J. E. Amonette, R. K. Kukkadapu, D. A. Schwartz and D. R. Gamelin, *J. Am. Chem. Soc.*, 2004, **126**, 9387.
8 M. A. Garcia, J. M. Merino, E. F. Pinel, A. Quesada, J. de la Venta, M. L. Ruız Gonzalez, G. R. Castro, P. Crespo, J. Llopis, J. M. Gonzalez-Calbet and A. Hernando, *Nano Lett.*, 2007, **7**, 1489.
9 J. Gao, J. M. Luther, O. E. Semonin, R. J. Ellingson, A. J. Nozik and M. C. Beard, *Nano Lett.*, 2011, **11**, 1002.
10 Y. J. Zeng, S. S. Lin, A. Volodin, Y. F. Lu, Z. Z. Ye and C. Van Haesendonck, *Appl. Phys. Lett.*, 2010, **97**, 143102.
11 A. P. Alivisatos, *Science*, 1996, **271**, 933.
12 C. Kittel, *Introduction to Solid State Physics*, Butterworth-Heinemann, 2005.
13 D. A. Muller, *Nat. Mater.*, 2009, **8**, 263.
14 P. M. Voyles, D. A. Muller, J. L. Grazul, P. H. Citrin and H.-J. L. Gossmann, *Nature*, 2002, **416**, 826.
15 S. Bals, S. Van Aert, C. P. Romero, K. Lauwaet, M. J. Van Bael, B. Schoeters, B. Partoens, E. Yücelen, P. Lievens and G. Van Tendeloo, *Nat. Commun.*, 2012, **1887**, 1.
16 L. Jdira, P. Liljeroth, E. Stoffels, D. Vanmaekelbergh and S. Speller, *Phys. Rev. B: Condens. Matter Mater. Phys.*, 2006, **73**, 115305.
17 P. Liljeroth, L. Jdira, K. Overgaag, B. Grandidier, S. Speller and D. Vanmaekelbergh, *Phys. Chem. Chem. Phys.*, 2006, **8**, 3845.
18 L. Jdira, K. Overgaag, J. Gerritsen, D. Vanmaekelbergh, P. Liljeroth and S. Speller, *Nano Lett.*, 2008, **8**, 4014.
19 U. Banin, Y. W. Cao, D. Katz and O. Millo, *Science*, 1999, **400**, 542.
20 T. Maltezopoulos, A. Bolz, C. Meyer, C. Heyn, W. Hansen, M. Morgenstern and R. Wiesendanger, *Phys. Rev. Lett.*, 2003, **91**, 196804.
21 D. A. Bonnel, *Prog. Surf. Sci.*, 1998, **57**, 187.

22 M. Wolovelsky, Y. Goldstein and O. Millo, *Phys. Rev. B: Condens. Matter Mater. Phys.*, 1998, **57**, 6274.
23 O. Dulub, U. Diebold and G. Kresse, *Phys. Rev. Lett.*, 2003, **90**, 016102.
24 O. Dulub, L. A. Boatner and U. Diebold, *Surf. Sci.*, 2002, **519**, 201.
25 K. Bromann, C. Felix, H. Brune, W. Harbich, R. Monot, J. Buttet and K. Kern, *Science*, 1996, **274**, 956.
26 S. Duffe, T. Irawan, M. Bieletzki, T. Richter, B. Sieben, C. Yin, B. von Issendorff, M. Moseler and H. Hövel, *Eur. Phys. J. D*, 2007, **45**, 401.
27 K. Sell, A. Kleibert, V. Von Oeynhausen and K.-H. Meiwes-Broer, *Eur. Phys. J. D*, 2007, **45**, 433.
28 K. Schouteden, A. Lando, E. Janssens, P. Lievens and C. Van Haesendonck, *New J. Phys.*, 2008, **10**, 083005.
29 W. H. Woodward, M. M. Blake, Z. Luo, P. S. Weiss and A. W. Castleman, Jr, *J. Phys. Chem. C*, 2011, **115**, 5373.
30 K. Lauwaet, K. Schouteden, E. Janssens, C. Van Haesendonck and P. Lievens, *Phys. Rev. B: Condens. Matter Mater. Phys.*, 2011, **83**, 155433.
31 E. V. Chulkov, M. Machado and V. M. Silkin, *Vacuum*, 2001, **61**, 95.
32 W. Bouwen, P. Thoen, F. Vanhoutte, S. Bouckaert, F. Despa, H. Weidele, R. E. Silverans and P. Lievens, *Rev. Sci. Instrum.*, 2000, **71**, 54.
33 K. Schouteden, P. Lievens and C. Van Haesendonck, *Phys. Rev. B: Condens. Matter Mater. Phys.*, 2009, **79**, 195409.
34 I. Horcas, R. Fernandez, J. M. Gomez-Rodriguez, J. Colchero, J. Gomez-Herrero and A. M. Baro, *Rev. Sci. Instrum.*, 2007, **78**, 013705.
35 M. Huijben, G. Rijnders, D. H. A. Blank, S. Bals, S. Van Aert, J. Verbeeck, G. Van Tendeloo, A. Brinkman and H. Hilgenkamp, *Nat. Mater.*, 2006, **5**, 556.
36 D. D. Chambliss, R. J. Wilson and S. Chang, *Phys. Rev. Lett.*, 1991, **66**, 1721.
37 Z. Y. Li, N. P. Young, M. Di Vece, S. Palomba, R. E. Palmer, A. L. Bleloch, B. C. Curley, R. L. Johnston, J. Jiang and J. Yuan, *Nature*, 2008, **451**, 46.
38 R. E. Palmer, S. Pratontep and H.-G. Boyen, *Nat. Mater.*, 2003, **2**, 443.
39 D. C. Look, J. W. Hemsky and J. R. Sizelove, *Phys. Rev. Lett.*, 1999, **82**, 2552.
40 A. Janotti and C. G. Van de Walle, *Nat. Mater.*, 2007, **6**, 44.
41 Y.-N. Xu and W. Y. Ching, *Phys. Rev. B: Condens. Matter Mater. Phys.*, 1993, **48**, 4335.
42 R. Wiesendanger, *Scanning Probe Microscopy and Spectroscopy: Methods and Applications*, Cambridge University Press, 1994.
43 L. Petersen, P. T. Sprunger, P. Hofmann, E. Lægsgaard, B. G. Briner, M. Doering, H.-P. Rust, A. M. Bradshaw, F. Besenbacher and E. W. Plummer, *Phys. Rev. B: Condens. Matter Mater. Phys.*, 1998, **57**, R6858, 7361.
44 G. Binnig, K. H. Frank, H. Fuchs, N. Garcia, B. Reihl, H. Rohrer, F. Salvan and A. R. Williams, *Phys. Rev. Lett.*, 1985, **55**, 991.
45 D. Steiner, D. Dorfs, U. Banin, F. D. Sala, L. Manna and O. Millo, *Nano Lett.*, 2008, **8**, 2954.
46 I. Swart, Z. Sun, D. Vanmaekelbergh and P. Liljeroth, *Nano Lett.*, 2010, **10**, 1931.
47 P. Sharma, A. Gupta, K. V. Rao, F. J. Owens, R. Sharma, R. Ahuja, J. M. O. Guillen, B. Johansson and G. A. Gehring, *Nat. Mater.*, 2003, **2**, 673.